Astron. Astrophys. 355, 1168–1180 (2000)

ASTRONOMY
AND
ASTROPHYSICS

Propagation effects in pulsar magnetospheres

S.A. Petrova and Y.E. Lyubarskii

Institute of Radio Astronomy, Chervonopraporna St.4, Kharkov, 61002 Ukraine

Received 7 June 1999 / Accepted 3 December 1999

Abstract. Refraction and polarization transfer in an ultrarelativistic highly magnetized pulsar plasma are considered. Normal waves in the pulsar plasma are linearly polarized however circular polarization arises in the polarization limiting region if radiation propagates at an angle to the plane of the magnetic field lines. The rays go off this plane due to refraction or (and) due to rotation of the magnetosphere. We found significant circular polarization of the outgoing radiation, in some cases with the sense reversal near the pulse centre. The frequency dependence of the circular polarization qualitatively resembles that observed. The swing of position angle of linear polarization is studied allowing for the wave propagation in the polarization-limiting region. The influence of refraction on the total-intensity profiles is examined as well. It is shown that refraction can provide the angular separation of emitted rays, so that the whole morphological classification of pulsar profiles can be explained within the frame of the primordial hollow-cone emission model taking into account wave propagation in the magnetosphere.

Key words: plasmas – polarization – waves – stars: pulsars: general

1. Introduction

Pulsar magnetospheres are believed to be filled with an ultrarelativistic electron-positron plasma. It streams along the open field lines of the dipolar magnetic field and ultimately leaves the magnetosphere. The plasma is supposed to give rise to radio emission. Although to date there is no commonly accepted mechanism of pulsar radio emission, it is clear that the emission of ultrarelativistic plasma should be highly directional. Narrowness and stability of the observed pulses imply that radio emission originates well within the magnetosphere, where the open field line tube is sufficiently narrow. Hence, the characteristics of the observed pulses should be conditioned by radio wave propagation in the magnetospheric plasma.

Given the axisymmetric distribution of the plasma number density, refraction of ordinary superluminous waves was found to be significant in pulsar magnetospheres (Barnard & Arons 1986; Lyubarskii & Petrova 1998). Ray deviation appears to occur mainly on account of the plasma density gradient across the open field line tube. With the distance from the neutron star the tube widens and the gradient decreases. Thus the efficiency of refraction is determined by the locus of the emission point. Provided that radiation of a given frequency is emitted at a corresponding radius (radius-to-frequency mapping) refraction should depend on the frequency. As shown by Lyubarskii & Petrova (1998), the characteristic features of the observed pulse width versus frequency curves can be explained in terms of refraction. In particular, refraction of waves in the open field line tube can naturally explain the so-called "absorption feature" observed in some pulsars.

As the waves are propagating through the magnetosphere their polarization also evolves essentially. The plasma embedded in a superstrong magnetic field allows two linearly polarized normal waves. One of them (the ordinary mode) is polarized in the same plane as the wave vector and the local magnetic field ($\mathbf{k} \times \mathbf{b}$ plane), while the other one (the extraordinary mode) is polarized perpendicularly to this plane. In the emission region, the scale length for beats between the normal waves is much less than the scale length for variation in the plasma parameters. So the normal waves propagate independently and their polarization plane is adjusted to the local orientation of the $\mathbf{k} \times \mathbf{b}$-plane. Since the plasma number density decreases with the distance from the neutron star, the scale length for beats increases along the trajectory. Ultimately the plasma density falls to an extent that the medium no longer affects wave propagation and the polarization becomes fixed. Thus the emergent polarization is conditioned by the evolution in the so-called polarization-limiting region, where geometrical optics fails. The normal waves then do not have enough time to follow the local orientation of the $\mathbf{k} \times \mathbf{b}$-plane and wave mode coupling takes place. This results in the elliptical polarization of the outgoing waves.

If the waves were propagating in the plane of the magnetic lines, wave mode coupling would not occur at all and polarization would remain unaltered along the trajectory. The wave mode coupling introduced by magnetosphere rotation was qualitatively considered by Cheng & Ruderman (1979) and Radhakrishnan & Rankin (1990). The quantitative treatment of the polarization transfer in the rotating magnetosphere was held by Lyubarskii & Petrova (1999). It was shown that the effect can account for the circular polarization observed in a number of pulsars in addition to the linear one.

von Hoesbroech, Lesch, Kunzl (1998) argue for another origin of the circularly polarized component of pulsar radio emission. These authors consider the plasma embedded in a finite magnetic field, the distribution functions for plasma electrons and positrons being taken different. Then the normal waves propagating at small angles to the magnetic field are circularly polarized, so that the circularly polarized component of pulsar radiation is explained by the dispersive properties of the magnetospheric plasma. However, well inside the magnetosphere the magnetic field strength is so high that the critical angle for the circularly polarized normal modes appear to be too small.

In the earlier literature there were a number of attempts to interpret the circular polarization of pulsar radiation as a characteristic of the emission mechanism (Bjornsson 1984; Michel 1987; Gil & Snakovski 1990a,b; Radhakrishnan & Rankin 1990; Gangadhara 1997). However, given that the open field line tube is filled with the plasma, the propagation effects cannot be omitted. Moreover, it is the wave propagation through the magnetosphere that sets up the polarization of outgoing radiation. Indeed, whatever the emission mechanism, only the normal waves allowed by the magnetospheric plasma can propagate and ultimately escape from pulsars.

It should be noted that the sense of circular polarization resulting from the wave mode coupling due to magnetosphere rotation is the same throughout the pulse. Such symmetric polarization profiles are really characteristic of a number of pulsars. However, polarization profiles of some other pulsars exhibit the sense reversal, which usually occurs near the pulse centre (see, e.g., Radhakrishnan & Rankin 1990; Han et. al. 1998). This phenomenon is commonly attributed to the peculiarities of the emission mechanism (see Radhakrishnan & Rankin 1990 and references therein).

The present paper suggests the interpretation of such antisymmetric profiles on the basis of propagation effects. Given that within the open field line tube the plasma is distributed nonuniformly in the azimuthal direction, refraction should cause ray deviation away from the initial magnetic line plane. Then the $\mathbf{k} \times \mathbf{b}$-plane turns along the trajectory and causes the polarization-limiting effect. It is shown that the wave mode coupling introduced by refraction in the plasma with nonaxisymmetric density distribution can explain the observed sense reversal in the profiles of circular polarization. Since refraction depends essentially on the locus of the ray origin and, in particular, on the polar angle of the emission point, significant amounts of circular polarization out of this effect can be achieved only in the vicinity of the magnetic axis.

As a rule, significant amounts of circular polarization resulting from the wave mode coupling are accompanied by a significant turn of the polarization ellipse. Indeed, the swing of the position angle observed in pulsars in the presence of a strong circular polarization does not correspond to the single-vector model (see, e.g., Rankin 1990).

The exhaustive analysis of a comprehensive observational material carried out by Rankin (1983) enabled her to assert that the emission from the central part of the open field line tube (core emission) is principally different from that generated at the tube edge (conal emission). Core and conal components of pulsar profiles were found to be quite distinct in both polarization and spectral properties. The present paper demonstrates that the characteristic features of pulsar polarization can be attributed to the propagation effects in the magnetosphere. Moreover, it is shown that the very existence of the separate components in total-intensity profiles and their frequency evolution can be regarded as a consequence of refraction in the magnetospheric plasma. We proceed from the fact that beyond the edge of the open field line tube as well as near the magnetic axis the plasma number density is negligible. So the plasma density is assumed to decrease towards the tube edge and towards the magnetic axis. Refraction is known to result in ray deviation in the direction of plasma density decrease. Hence, the rays emitted near the inner boundary of the plasma flow deviate towards the magnetic axis and can be recognized as core emission, whereas the rays emitted near the outer tube edge deviate away from the magnetic axis and form conal components. At high frequencies refraction is more efficient and component separation should become more prominent. Thus there is no need to involve two distinct mechanisms to explain core and conal emission. The properties of pulsar integrated profiles can be well interpreted in terms of the common hollow-cone model with allowance for the propagation effects.

In Sect. 2 general equations describing refraction and polarization transfer are deduced. Sect. 3 contains numerical results and their discussion. In Sect. 3.1 the circular polarization profile with the sense reversal is obtained. Its frequency evolution is considered as well. Symmetrical profiles of circular polarization are investigated in Sect. 3.2. The lack of circular polarization in conal components is also discussed there. In Sect. 3.3 position angle swing in the presence of strong circular polarization is examined. In Sect. 3.4 it is shown how refraction can cause the angular separation of the components in total-intensity profiles. The frequency evolution of such profiles is analysed as well. The results are summarized in Sect. 4.

2. General equations

2.1. Refraction in plasma with nonaxisymmetric density distribution

General theory of refraction in pulsar magnetosphere was first developed by Barnard & Arons (1986). The equations obtained were applied to the case of an axisymmetric plasma density distribution. Now we are to examine refraction in the more general case of nonaxisymmetric density distribution. Let us consider an ultrarelativistic highly magnetized electron-positron plasma, which is cold in the proper rest frame. The dispersion relation for ordinary waves in such a plasma is known to be the following (see, e.g., review by Lyubarskii 1995):

$$\left(1 - n_{\parallel}^2\right)\left(1 - \frac{\omega_p^2}{\omega^2\gamma^3(1 - n_{\parallel}\beta)^2}\right) - n_{\perp}^2 = 0. \qquad (1)$$

Here γ is the plasma Lorentz-factor, β the plasma velocity in units of c, $n_{\parallel} = ck_{\parallel}/\omega$, $n_{\perp} = ck_{\perp}/\omega$, with $k_{\parallel}$, $k_{\perp}$ being

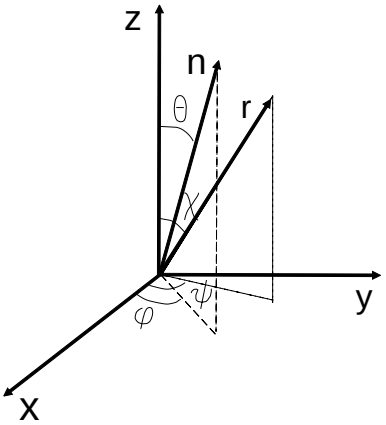

Fig. 1. The vectors **n** and **r** in the coordinate system considered in the text

the wave vector components along and perpendicularly to the magnetic field, correspondingly, ω_p is the plasma frequency given by the customary expression:

$$\omega_p = \sqrt{\frac{4\pi N e^2}{m}}, \tag{2}$$

where N is the plasma number density, m the electron mass. Eq. (1) yields two ordinary normal waves. One of them is subluminous and therefore does not escape from the magnetosphere because of Landau damping. The extraordinary wave has the vacuum dispersion law and, consequently, is not affected by refraction. So we are interested only in the ordinary superluminous wave.

Since the characteristic scale lengths of the open field line tube are much larger than the wavelength, geometrical optics approximation is valid. Wave propagation then can be described by Hamilton's equations, which take the form (Barnard & Arons 1986):

$$\frac{1}{c}\frac{d\mathbf{r}}{dt} = p\mathbf{n} - q\mathbf{b},$$

$$\frac{1}{\omega}\frac{d\mathbf{k}}{dt} = q\frac{\partial \mathbf{b}}{\partial \mathbf{r}}\cdot\mathbf{n} - l\frac{\partial \ln N}{\partial \mathbf{r}}, \tag{3}$$

where **n** and **b** are the unit vectors aligned with the wave vector and magnetic field, respectively,

$$p = (1+\eta)^3/d, \quad q = 4(1-\eta)/(f^2 d),$$

$$l = 2(1+\eta)(1-n_\parallel^2)/(f^2 d), \quad \eta = 2\gamma^2(1-n_\parallel),$$

$$d = (1+\eta)^3 - 4(1-\eta)(1-\eta/(2\gamma^2))/f^2,$$

$$f = \frac{\omega}{\omega_p\sqrt{\gamma}}. \tag{4}$$

The magnetic field is supposed to be dipolar. Let (r, χ, ψ) be the spherical coordinates in the system with the polar axis directed along the magnetic axis (see Fig. 1). The Cartesian components of **b** can be written as

$$b_x = \frac{3}{2}\chi\cos\psi, \quad b_y = \frac{3}{2}\chi\sin\psi. \tag{5}$$

Here it is taken into account that the open field line tube is narrow, so that the polar angle χ is small. Let the vector **n** make the angle θ with the z-axis and the plane containing **n** and the z-axis makes the angle φ with the x-axis. Given that the ray is emitted along the magnetic line the angle θ is expected to be of the order of χ all over the trajectory. Then one can reduce Eq. (3) to the form:

$$\frac{1}{c}\frac{dr}{dt} = pn_\parallel - q,$$

$$\frac{r}{c}\frac{d\chi}{dt} = pn_\parallel\theta\cos(\varphi-\psi) - \chi p n_\parallel - \frac{\chi q}{2},$$

$$\frac{r\chi}{c}\frac{d\psi}{dt} = pn_\parallel\theta\sin(\varphi-\psi),$$

$$\frac{1}{c}\frac{dn_\parallel}{dt} = -l\frac{\partial\ln N}{\partial r} + \frac{l\chi}{r}\frac{\partial\ln N}{\partial\chi}, \tag{6}$$

$$\frac{n_\parallel}{c}\frac{d\theta}{dt} = \frac{3qn_\parallel}{2r}\left[\theta - \frac{3}{2}\chi\cos(\varphi-\psi)\right]$$

$$-\frac{l\cos(\varphi-\psi)}{r}\frac{\partial\ln N}{\partial\chi} + \frac{l\sin(\psi-\varphi)}{r\chi}\frac{\partial\ln N}{\partial\psi}$$

$$-l\frac{\partial\ln N}{\partial r}\left[\chi\cos(\psi-\varphi) - \theta\right],$$

$$\frac{n_\parallel\theta}{c}\frac{d\varphi}{dt} = -\frac{9q}{4r}\chi n_\parallel\sin(\psi-\varphi)$$

$$-\frac{l\sin(\psi-\varphi)}{r}\frac{\partial\ln N}{\partial\chi} - \frac{l\cos(\psi-\varphi)}{r\chi}\frac{\partial\ln N}{\partial\psi}$$

$$-l\chi\sin(\psi-\varphi)\frac{\partial\ln N}{\partial r}.$$

For the sake of simplicity one can eliminate the time dependence dividing the system equations by the first one and replace one of them by the dispersion relation (1). Then we find finally:

$$r\frac{d\chi}{dr} = \frac{1}{pn_\parallel - q}\left[\frac{3}{2}pn_\parallel\theta\cos(\varphi-\psi) - \chi p n_\parallel - \frac{\chi q}{2}\right],$$

$$r\chi\frac{d\psi}{dr} = \frac{3}{2}\frac{pn_\parallel\theta}{pn_\parallel - q}\sin(\varphi-\psi),$$

$$n_\parallel\frac{d\theta}{dr} = \frac{1}{pn_\parallel - q}\left\{\frac{3qn_\parallel}{2r}\left[\theta - \chi\cos(\varphi-\psi)\right]\right.$$

$$-\frac{2l\cos(\psi-\varphi)}{3r\chi_0^2}\frac{\partial \ln N}{\partial \chi}+\frac{2l\sin(\psi-\varphi)}{3r\chi\chi_0^2}\frac{\partial \ln N}{\partial \psi}$$

$$-l\frac{\partial \ln N}{\partial r}\left[\frac{2}{3}\chi\cos(\psi-\varphi)-\theta\right]\Bigg\}, \qquad (7)$$

$$n_\parallel\theta\frac{d\varphi}{dr}=\frac{1}{pn_\parallel-q}\left[-\frac{3q}{2r}\chi n_\parallel\sin(\psi-\varphi)\right.$$

$$-\frac{2l\sin(\psi-\varphi)}{3r\chi_0^2}\frac{\partial \ln N}{\partial \chi}-\frac{2l\cos(\psi-\phi)}{3r\chi\chi_0^2}\frac{\partial \ln N}{\partial \psi}$$

$$\left.-\frac{2}{3}l\chi\sin(\psi-\varphi)\frac{\partial \ln N}{\partial r}\right],$$

$$\eta\left(1-\frac{4N}{f_0^2r^3(1+\eta)^2}\right)$$

$$-\frac{9}{4}\chi_0^2\gamma^2\left[\theta^2+\chi^2-2\chi\theta\cos(\psi-\varphi)\right]=0.$$

Here the quantities r, χ, θ, N are normalized by their initial values and it is taken into account that $\theta_0=3\chi_0/2$; the subscript "0" refers to the initial values. The set of Eqs. (7) describes the wave vector evolution and the trajectory of the ordinary superluminous waves in an ultrarelativistic highly magnetized plasma with nonaxisymmetric density distribution.

2.2. Polarization transfer in pulsar magnetosphere

Now let us consider the polarization evolution along the wave trajectory within the rotating pulsar magnetosphere (for more details see Lyubarskii & Petrova 1999). The wave fields E and B are described by Maxwell's equations:

$$\nabla\times\mathbf{B}=-\frac{i\omega}{c}\mathbf{E}+\frac{4\pi}{c}\mathbf{j}_1,$$

$$\nabla\times\mathbf{E}=\frac{i\omega}{c}\mathbf{B}, \qquad (8)$$

$$-i\omega e(n_1^+-n_1^-)+\mathrm{div}\mathbf{j}_1=0.$$

Here $\mathbf{j}_1$ is the linearized current density caused by the wave,

$$\mathbf{j}_1\equiv e[\mathbf{v}_0(n_1^+-n_1^-)+n_0(\mathbf{v}_1^+-\mathbf{v}_1^-)],$$

$\mathbf{v}_0$ and n_0 are respectively the velocity and number density unperturbed by the wave, $\mathbf{v}_1^\pm$ and $n_1^\pm$ the small perturbations of these quantities for electrons and positrons. Note that in our consideration the slight difference in the unperturbed values of $\mathbf{v}_0$ and n_0 for electrons and positrons can be neglected.

The plasma is assumed to be cold. The plasma particle motion in the infinitely strong magnetic field can be examined in terms of the mechanical bead-on-a-wire model: the particles are constrained to move along the magnetic lines, which rotate at the angular velocity $\mathbf{\Omega}$. To the first order in $|\mathbf{\Omega}\times\mathbf{r}|/c$ the equation of plasma particle motion can be written as:

$$m\gamma^3\frac{dv_b^\pm}{dt}=\pm e\left[\mathbf{E}+\frac{(\mathbf{\Omega}\times\mathbf{r})\times\mathbf{B}}{c}\right]\cdot\mathbf{b}, \qquad (9)$$

where $v_b^\pm$ is the velocity along the magnetic line for electrons and positrons. Note that the left-hand side of Eq. (9) contains the total derivative, $\frac{d}{dt}\equiv-i\omega+\mathbf{v}_0\cdot\nabla$.

We are particularly interested in polarization transfer in the so-called polarization-limiting region, where geometrical optics fails and

$$\frac{\omega}{c}\Delta n\cdot s\sim 1; \qquad (10)$$

here Δn is the difference between the refractive indices of the extraordinary and ordinary waves, s the characteristic scale length for change in the plasma parameters; it is expected that $s\sim r_p$, with r_p being the polarization-limiting radius. At distances $\sim r_p$ the refractive index of the ordinary wave differs from unity by $\frac{c}{\omega r_p}\ll 1$, while the extraordinary wave is the vacuum electromagnetic one. Consequently, in the polarization-limiting region one can neglect refraction and consider the wave propagation as a straight-line.

Let us choose the three-dimensional Cartesian system with the z-axis along the wave vector. Then all the perturbed quantities should depend only on the z-coordinate. Hence, Eqs. (8) and (9) can be rewritten as follows:

$$\frac{d^2E_x}{dz^2}+\frac{\omega^2}{c^2}E_x+\frac{4\pi i\omega}{c^2}\left[j_b b_x+e\left(n_1^+-n_1^-\right)(\mathbf{\Omega}\times\mathbf{r})_x\right]=0,$$

$$\frac{d^2E_y}{dz^2}+\frac{\omega^2}{c^2}E_y+\frac{4\pi i\omega}{c^2}\left[j_b b_y+e\left(n_1^+-n_1^-\right)(\mathbf{\Omega}\times\mathbf{r})_y\right]=0,$$

$$\frac{\omega^2}{c^2}E_z+\frac{4\pi i\omega}{c^2}\left[j_b b_z+e\left(n_1^+-n_1^-\right)(\mathbf{\Omega}\times\mathbf{r})_z\right]=0, \qquad (11)$$

$$-i\omega e(n_1^+-n_1^-)+b_z\frac{dj_b}{dz}+e(\mathbf{\Omega}\times\mathbf{r})_z\frac{d(n_1^+-n_1^-)}{dz}=0,$$

$$\frac{m\gamma^3}{en_0}\left\{-i\omega[j_b-ev_b(n_1^+-n_1^-)]+[v_b b_z+(\mathbf{\Omega}\times\mathbf{r})_z]\right.$$

$$\left.\cdot\left[\frac{dj_b}{dz}-ev_b\frac{d(n_1^+-n_1^-)}{dz}\right]\right\}$$

$$=2e\left\{E_x b_x+E_y b_y+E_z b_z+\frac{ic}{\omega}\left(q_x\frac{dE_y}{dz}-q_y\frac{dE_x}{dz}\right)\right\},$$

where

$$j_b\equiv e[v_b(n_1^+-n_1^-)+n_0(v_1^+-v_1^-)],$$

$$\mathbf{q}\equiv\frac{\mathbf{b}\times(\mathbf{\Omega}\times\mathbf{r})}{c}.$$

Above it is taken into account that the scale length for change in the unperturbed medium parameters $\mathbf{b}$, $\mathbf{v}_0$ and n_0 is much larger than the wavelength.

As the refractive indices are very close to unity, the perturbed quantities corresponding to the wave propagating in the positive direction of the z-axis can be presented in the form:

$$E_{x,y,z} = a_{x,y,z}(z)\exp(i\frac{\omega}{c}z),$$

$$j_b = a_j(z)\exp(i\frac{\omega}{c}z),$$

$$n_1^+ - n_1^- = a_n(z)\exp(i\frac{\omega}{c}z),$$

with $a(z)$ being the slowly varying amplitudes:

$$\frac{da}{dz} \ll \frac{a\omega}{c}.$$

Using the above condition one can rewrite Eq. (11) as

$$\frac{da_x}{dz} + \frac{2\pi}{c}[a_j b_x + e a_n(\mathbf{\Omega}\times\mathbf{r})_x] = 0,$$

$$\frac{da_y}{dz} + \frac{2\pi}{c}[a_j b_y + e a_n(\mathbf{\Omega}\times\mathbf{r})_y] = 0,$$

$$a_z + \frac{4\pi i}{\omega}[a_j b_z + e a_n(\mathbf{\Omega}\times\mathbf{r})_z] = 0,$$

$$e a_n\left[1 - \left(\frac{\mathbf{\Omega}\times\mathbf{r}}{c}\right)_z\right] - \frac{a_j}{c}b_z = 0, \qquad (12)$$

$$-i\omega(a_j - e v_b a_n)\left[1 - \frac{v_b}{c}b_z - \left(\frac{\mathbf{\Omega}\times\mathbf{r}}{c}\right)_z\right]$$

$$= \frac{2e^2 n_0}{m\gamma^3}[E_x(b_x+q_y) + E_y(b_y - q_x) + E_z b_z].$$

It should be noted that the waves considered are quasi-transverse ones, since their refractive indices are very close to unity, so that the z-component of the wave electric field is small, $a_z \ll a_x$, a_y. Then the set (12) can be easily reduced to the form:

$$\frac{da_x}{dz} = -iR\left[(b_x+q_y)^2 a_x + (b_x+q_y)(b_y-q_x)a_y\right],$$

$$\frac{da_y}{dz} = -iR\left[(b_x+q_y)(b_y-q_x)a_x + (b_y-q_x)^2 a_y\right], \qquad (13)$$

where

$$R \equiv \frac{\omega_p^2}{2\omega c\gamma^3(1-\beta_z)^2},$$

with $\omega_p \equiv \sqrt{8\pi n_0 e^2/m}$ being the plasma frequency, β_z the z-component of the plasma velocity in units of c.

As long as $Rz \gg 1$ Eq. (13) can be treated in terms of geometrical optics. Then it is not difficult to find that in the corotating frame wave polarization follows the local orientation of the $\mathbf{k}\times\mathbf{b}$-plane. It is quite what Cheng & Ruderman (1979) called the 'adiabatic walking'. These authors examined qualitatively polarization evolution in a narrow beam of rays, which is initially centered on a magnetic line. At the emission point the average polarization of the beam is zero. However, further along the trajectory the beam axis deviates from the magnetic field vector because of field line curvature. This was shown to result in ordering the polarization angles of beam rays, which ultimately leads to an almost complete average beam polarization. Taking into account this fact, we shall consider only the waves emitted along the magnetic field. Note that we allowed for the aberration because of magnetosphere rotation (the vector $\mathbf{q}$).

Since the plasma density decreases along the wave trajectory, geometrical optics is ultimately violated. Obviously, in the opposite limiting case, $Rz \ll 1$, the wave amplitudes remain constant. For a more detailed discussion of the characteristic features of polarization transfer on the basis of Eq. (13) see Lyubarskii & Petrova (1999).

To proceed further we consider the polarization-limiting effect for the ordinary waves assuming that due to refraction in the vicinity of the emission region waves propagate at an angle to the plane of the magnetic lines. It should be noted that, in agreement with the definition (10), refraction is negligible in the polarization-limiting region. On the other hand, near the emission region geometrical optics approximation is appropriate, so that polarization evolution is known. Thus the problems on refraction and polarization transfer can be treated separately.

Let the coordinates of the wave packet after a sufficient cease of refraction be r_f, χ_f, ψ_f, the wave vector make the angle θ_f with the z-axis and the projection of $\mathbf{n}$ on the equatorial plane make the angle φ_f with the x-axis. Further along the ray trajectory, at larger altitudes in the magnetosphere, rotational effects become essential. The spherical coordinate system spoken about is assumed to be chosen in such a way that initially the polar axis is directed along the magnetic axis and the fiducial direction in the equatorial plane is that opposite to the projection of the rotation axis (see Fig. 2). Now we turn to the Cartesian system with the z-axis along the final direction of the wave vector and the xz-plane initially containing the magnetic axis. The Cartesian components of the vector $\mathbf{b}$ in each point of the wave trajectory can be found to be:

$$b_x = \frac{3}{2u}\chi_f\cos(\psi_f - \varphi_f) + \frac{3}{2}\frac{u-1}{u}\theta_f - \theta_f - \frac{\Omega t}{2}\sin\alpha\sin\varphi,$$

$$b_y = \frac{3}{2u}\chi_f\sin(\psi_f - \varphi_f) - \frac{\Omega t}{2}\sin\alpha\cos\varphi, \qquad (14)$$

where α is the angle between the magnetic and rotation axes, $u \equiv r/r_f$, $t \equiv (r-r_f)/c$. Above it is taken into account that well within the light cylinder $\Omega t \ll 1$. The components of the vector $\mathbf{q}$ can be written as:

$$q_x = -\frac{\Omega r}{c}\sin\alpha\cos\varphi, \quad q_y = \frac{\Omega r}{c}\sin\alpha\sin\varphi. \qquad (15)$$

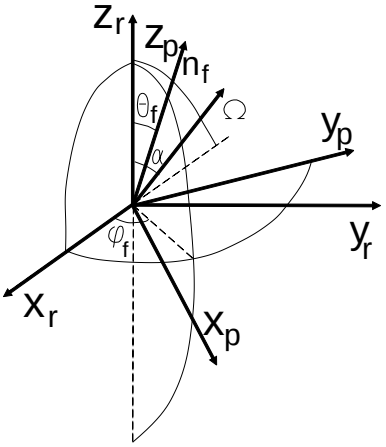

Fig. 2. Relative orientation of the axes of the coordinate systems used in the text to describe refraction and polarization evolution of the wave packet. The rotational axis and final wave vector orientation are plotted as well. The ray trajectory and wave vector deviation on account of refraction are considered in the system $X_rY_rZ_r$, while polarization evolution is evaluated in the $X_pY_pZ_p$-system. Both systems are fixed in space and initially the magnetic axis is aligned with the z_p-axis

Provided that in Eqs. (14)–(15) the rotation effect as well as the influence of refraction are ignored (i.e., $\psi_f = \vartheta_f$ and $\Omega = 0$) the equations of the set (13) are not coupled, so that the normal waves propagate independently throughout the trajectory. Polarization-limiting effect occurs on account of the $\mathbf{k} \times \mathbf{b}$-plane turn along the wave trajectory. The ray can deviate from the initial magnetic line plane because of refraction in the plasma with nonaxisymmetric density distribution and also because of magnetosphere rotation. Given that the azimuthal distribution of the plasma density has an extremum, the rays emitted on the opposite sides of the extremum should deviate in the opposite directions due to oppositely directed density gradient. Consequently, their $\mathbf{k} \times \mathbf{b}$-planes turn in opposite directions, so that the circular polarization because of the wave mode coupling should reverse the sense during the pulse. Provided that refraction is strong ray trajectories curve intensely and quickly escape from the region filled with the plasma, so that magnetosphere rotation does not affect polarization evolution. Refraction is known to be significant at high frequencies. For the lower frequencies, which are supposed to originate at larger distances, refraction ceases, whereas the rotation effect becomes essential. Thus the wave mode coupling introduced by refraction and by magnetosphere rotation can be treated separately. Note that magnetosphere rotation causes the circular polarization of the sense constant throughout the pulse (Cheng & Ruderman 1979; Radhakrishnan & Rankin 1990).

3. Observational consequences of propagation effects

3.1. Wave mode coupling introduced by refraction

According to the standard models of electron-positron cascade, close to the magnetic axis as well as beyond the edge of the open field line tube the plasma density is negligible. So we assume that the plasma is distributed in the tube in such a way that the region near the magnetic axis constrained by characteristic open magnetic lines is free from the plasma. As the distance from the neutron star increases, the open field lines diverge and the plasma flow widens. In addition, the plasma density distribution is expected to be nonaxisymmetric (Arons & Scharlemann 1979). In agreement with the above considerations, we choose the following distribution of the plasma number density:

$$N = \begin{cases} N_0 \left(\frac{r_0}{r}\right)^3 \frac{\chi - \chi_1\sqrt{r/r_0}}{(\chi_2 - \chi_1)\sqrt{r/r_0}} \\ \times \exp(-\sin^2\psi), \quad \chi_1\sqrt{r/r_0} \le \chi \le \chi_2\sqrt{r/r_0}, \\ 0, \qquad \chi < \chi_1\sqrt{r/r_0} \quad \text{and} \quad \chi > \chi_2\sqrt{r/r_0}. \end{cases} \tag{16}$$

Recall that r_0 is radius of the emission point, which is assumed to be well within the light cylinder. Taking into account that

$$\frac{\partial \ln N}{\partial r} = -\frac{3}{r} - \frac{1}{2r}\frac{\chi}{\chi - \chi_1\sqrt{r}},$$

$$\frac{\partial \ln N}{\partial \chi} = \frac{1}{\chi - \chi_1\sqrt{r}},$$

$$\frac{\partial \ln N}{\partial \psi} = -2\sin\psi\cos\psi$$

and recalling the definitions (4) one can rewrite the set of Eqs. (7) in the following form:

$$r\frac{d\chi}{dr} = \frac{\chi}{2} + \frac{3(1+\eta)^3}{2A}\left[\theta\cos(\varphi - \psi) - \chi\right],$$

$$r\chi\frac{d\psi}{dr} = \frac{3(1+\eta)^3\theta}{2A}\sin(\varphi - \psi),$$

$$\frac{d\theta}{dr} = \frac{6(1-\eta)N}{Arf_0^2}\left[\theta - \chi\cos(\varphi - \psi)\right] - \frac{4(1+\eta)\eta N}{3Arf_0^2\chi_0^2\gamma^2}$$

$$\times \left[\frac{\cos(\varphi - \psi)}{\chi - \chi_1\sqrt{r}} + \frac{2\sin(\psi - \varphi)\sin\psi\cos\psi}{\chi}\right], \tag{17}$$

$$\theta\frac{d\varphi}{dr} = -\frac{6(1-\eta)N\chi}{Arf_0^2}\sin(\psi - \varphi)$$

$$-\frac{4\eta(1+\eta)N}{3Arf_0^2\chi_0^2\gamma^2}\frac{\sin(\psi - \varphi)}{\chi - \chi_1\sqrt{r}}$$

$$+\frac{8\eta(1+\eta)N}{9Arf_0^2\chi\chi_0^2\gamma^2}\cos(\psi - \varphi)\sin\psi\cos\psi,$$

$$\eta\left(1 - \frac{4N}{f_0^2r^3(1+\eta)^2}\right)$$

$$-\frac{9}{4}\chi_0^2\gamma^2\left[\theta^2 + \chi^2 - 2\chi\theta\cos(\varphi - \psi)\right] = 0.$$

Here

$$A \equiv (1+\eta)^3 - \frac{4(1-\eta)N}{f_0^2},$$

the quantities r, χ, θ, N are normalized by their initial values and the terms of the order of χ^2 are neglected. Provided that $\chi_0\gamma \lesssim 1$ the rays suffer strong deviation towards the magnetic axis and ultimately enter the region containing no plasma. The polarization-limiting region, where refraction is already insignificant, but the influence of the medium on wave propagation is still essential, should lie near the inner edge of the plasma flow at distances $r_p \sim r_0$ from the neutron star. Hence, neglecting magnetosphere rotation is really a good approximation in the case considered.

We assume that initially radiation is emitted along the magnetic field. Solution of Eqs. (17) yields direction of the outgoing wave, θ_f and φ_f. Then we solve Eqs. (13) and find the final polarization of this wave. The final circular polarization of outgoing waves can be characterized by the normalized Stokes parameter V:

$$V \equiv \frac{i(a_y a_x^* - a_x a_y^*)}{a_x a_x^* + a_y a_y^*}. \tag{18}$$

It is easy to show (e.g., see Fig. 10.4 in Manchester & Taylor 1977) that the rays detectable by an observer should satisfy the following relation:

$$\tan\varphi_f = \pm\sqrt{\frac{\theta_f^2}{(\alpha-\xi)^2} - 1}, \tag{19}$$

where ξ is the wave vector tilt to the rotation axis. The pulse phase, Φ, is then given by the expression:

$$\Phi = \frac{\tan\varphi_f}{\sin\alpha}(\alpha - \xi). \tag{20}$$

Since the rays deviate on account of refraction, one cannot know in advance what initial conditions correspond to the rays detected by an observer. So to find the pulse profile we traced the wave vector evolution for the rays emitted all over the open field line tube and then chose those satisfying Eq. (19) to calculate the final polarization. The profiles of circular polarization obtained through numerical solution of Eqs. (17) and (13) are presented in Fig. 3. It is clear that the wave mode coupling introduced by refraction in the plasma with the number density Eq. (16) can produce significant circular polarization. The polarization profiles appear to be antisymmetric, with the sense of circular polarization being changed at the pulse centre. In agreement with the fourth equation of the set (7), it is the azimuthal density gradient that causes the wave vector deviation away from the initial field line plane, the direction of the deviation being opposite to the gradient. Then the change in the sign of the azimuthal density gradient leads to the corresponding change in the sign of the $\mathbf{k}\times\mathbf{b}$-plane turn, so that the resulting circular polarization reverses the sense. With the density distribution Eq. (16), the sense reversal occurs at the pulse centre. Note that only the extremums projected near the pulse centre can cause the observable sense reversal. The point is that refraction is essential only for the rays close enough to the magnetic axis, $\theta\gamma \sim \chi_0\gamma \lesssim 1$. Note that although the rays deviate intensely given $\chi_0\gamma \lesssim 1$, the wave mode coupling introduced by refraction can be efficient at the weaker condition, $\chi_0\gamma \gtrsim 1$ as well, so that the width of the antisymmetrical region of the profile appears to be compatible with that observed. The polarization profiles shown in Fig. 3 are similar to those observed for a number of pulsars (see, e.g., Han

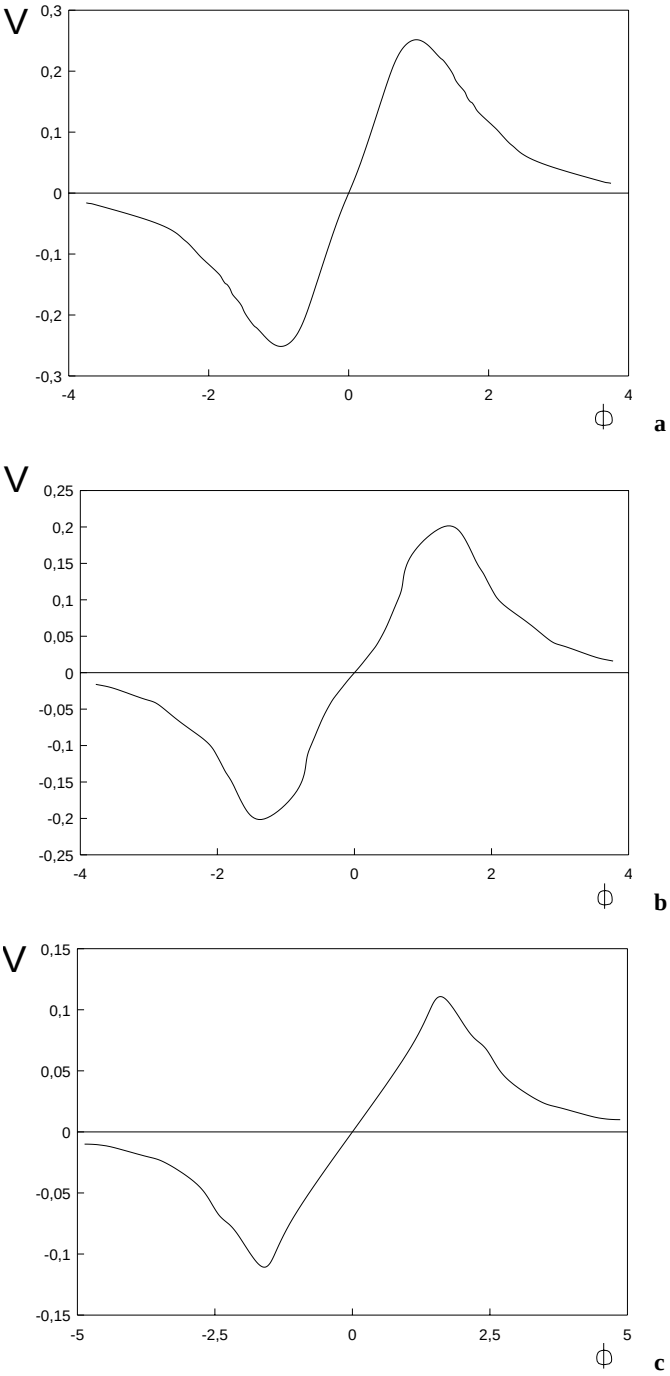

Fig. 3. Profiles of circular polarization resulting from the wave mode coupling introduced by refraction in the plasma with nonaxisymmetric density distribution: **a** $\chi_1 = 0.0015$, **b** $\chi_1 = 0.0025$, **c** $\chi_1 = 0.0075$; $\gamma = 50$, $f_0 = 0.5$, $\alpha = 0.5$, $\xi - \alpha = 0.0035$, $\frac{\omega r_f}{c\gamma^2} = 100$, $\chi_2 = 10\chi_1$

et. al. 1998 and references therein). The sense reversal is really observed only near the pulse centre.

One more issue worth discussion is the frequency evolution of such profiles. Let us suppose that the waves are emitted at frequencies of the order of the characteristic plasma frequency, $\omega \sim \omega_{p0}\sqrt{\gamma}$. Because the plasma flow widens with the distance, $N \propto r^{-3}$, each frequency originates at a corresponding radius, $\nu \propto r^{-3/2}$. Open field lines of the dipolar magnetic field diverge with the distance so that for a chosen magnetic line $\chi \propto \sqrt{r}$. As obvious from Eq. (17), the efficiency of refraction is determined by the factor $(\chi_0\gamma)^{-2}$. Hence, with the distance from the neutron star refraction becomes less efficient and, correspondingly, wave mode coupling ceases. Thus, the lower the frequency the smaller amounts of circular polarization are achievable. This trend is demonstrated in Fig. 3, where the curves are obtained for the case, when the polar angles χ_1 of the boundary magnetic line are related to each other as $3:5:15$, that is, the frequency ratio is $37:8:0.3$. Such frequency evolution of the antisymmetric polarization profiles is compatible with the observed one (see, e.g., the frequency sets of V-profiles for PSR 1451-68 and PSR 1857-26 in Rankin 1983).

Another striking observational fact is that at sufficiently low frequencies these antisymmetrical profiles can turn into symmetrical ones; then the sense of circular polarization becomes the same all over the pulse, save that the nulling of V and small amounts of the reverse polarization can be met in the wings of the pulse. So the circular polarization profile of PSR 1859+03 given by Radhakrishnan & Rankin (1990) as an example of the antisymmetric species ($\nu = 1412$ MHz) appears to be symmetrical at the frequencies 631 MHz (McCulloch et. al. 1978) and 430 MHz (Rankin & Benson 1981). Similarly, the V-profile of PSR 1917+00, which is antisymmetric at $\nu = 1400$ MHz (Rankin et. al. 1989), becomes symmetrical at $\nu = 430$ MHz (Rankin & Benson 1981). This testifies for the fact that at low frequencies the wave mode coupling introduced by refraction is dominated by that introduced by magnetosphere rotation.

3.2. Wave mode coupling introduced by magnetosphere rotation

For the sake of simplicity let us consider the axisymmetric distribution of the plasma density. Then refraction does not contribute to the turn of the $\mathbf{k}\times\mathbf{b}$-plane along the trajectory and wave mode coupling occurs only on account of magnetosphere rotation. Let

$$N=\begin{cases} N_0\left(\frac{r_0}{r}\right)^3 \frac{\chi-\chi_1\sqrt{r/r_0}}{(\chi_c-\chi_1)\sqrt{r/r_0}}, & \chi_1\sqrt{r/r_0}\le\chi\le\chi_c\sqrt{r/r_0},\\ N_0\left(\frac{r_0}{r}\right)^3 \frac{\chi_2\sqrt{r/r_0}-\chi}{(\chi_2-\chi_c)\sqrt{r/r_0}}, & \chi_c\sqrt{r/r_0}\le\chi\le\chi_2\sqrt{r/r_0},\\ 0, & \chi<\chi_1\sqrt{r/r_0} \quad\text{and}\quad \chi>\chi_2\sqrt{r/r_0}, \end{cases} \tag{21}$$

that is the plasma is confined between the two open field lines and the density decreases towards both boundaries. The set of equations describing refraction can be easily obtained from Eq. (17) putting $\psi=\varphi$ and replacing χ_1 by χ_2 for the region of outward density decrease. Numerical solution of Eqs. (17) and (13) then yields almost symmetrical profile of circular polarization shown in Fig. 4. Apparently, the wave mode coupling introduced by the magnetosphere rotation can result in significant amounts of circular polarization, so that the highest observed $|V|$, $\sim 60\%$ for PSR 1702-19 (Biggs et. al. 1988), can be explained by the effect. The sense of the circular polarization remains the same throughout the pulse. The polarization profile in Fig. 4 exhibits a slight departure from the symmetrical shape. The matter is that rotation of the open field line tube breaks the symmetry in wave propagation at negative and positive azimuths.

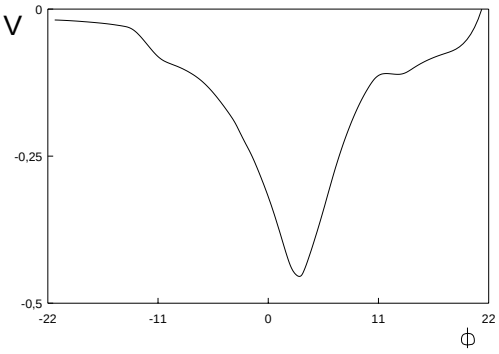

Fig. 4. The profile of circular polarization resulting from the wave mode coupling introduced by magnetosphere rotation; $\gamma=50$, $f_0=0.5$, $\alpha=0.5$, $\xi-\alpha=0.048$, $r_f/r_L=0.02$, $\frac{\omega r_f}{c\gamma^2}=100$, $\chi_1=0.01$, $\chi_c=7\chi_1$, $\chi_2=10\chi_1$

As can be seen from Eq. (13), the sign of V should depend on the signs of b_x and b_y. According to Eq. (14), the component b_y is purely determined by the magnetosphere rotation, the sign being the same all over the pulse. Now we are to examine the behaviour of the component b_x. As clear from Eq. (14), if magnetosphere rotation is sufficiently slow and the ray emitted along the open field line is not affected by refraction, that is, $3\chi_f/2=\theta_f$, b_x remains positive in each point of the trajectory. Given that refraction causes ray deviation towards the magnetic axis, $\theta_f<3\chi_f/2$, b_x is all the more positive. Strong enough outward deviation of the ray, however, can provide negative values of the component b_x in the vicinity of the starting point of straight-line propagation ($u\sim 1$), while at larger distances, $u\gg 1$, b_x becomes positive because of the magnetic line curvature. Hence, if refraction is strong and polarization-limiting radius lies not too far from the emission region, $r_p/r_f\sim 1$, the waves deviating away from the magnetic axis should gain the circular polarization of the sense opposite to that resulting from the wave mode coupling in case of wave deviation towards the axis. Note that if refraction outwards the axis is slightly weaker or r_p is located slightly further, b_x changes sign at $r<r_p$, so that the wave has enough time to start acquiring the circular polarization of another sense. Obviously, this can lead to an essential decrease in the emergent circular polarization. The above considerations are illustrated in Fig. 5. Take note of the sense reversal and depolarization at the wings of the profiles. It should be pointed out that both the peculiarities are confirmed

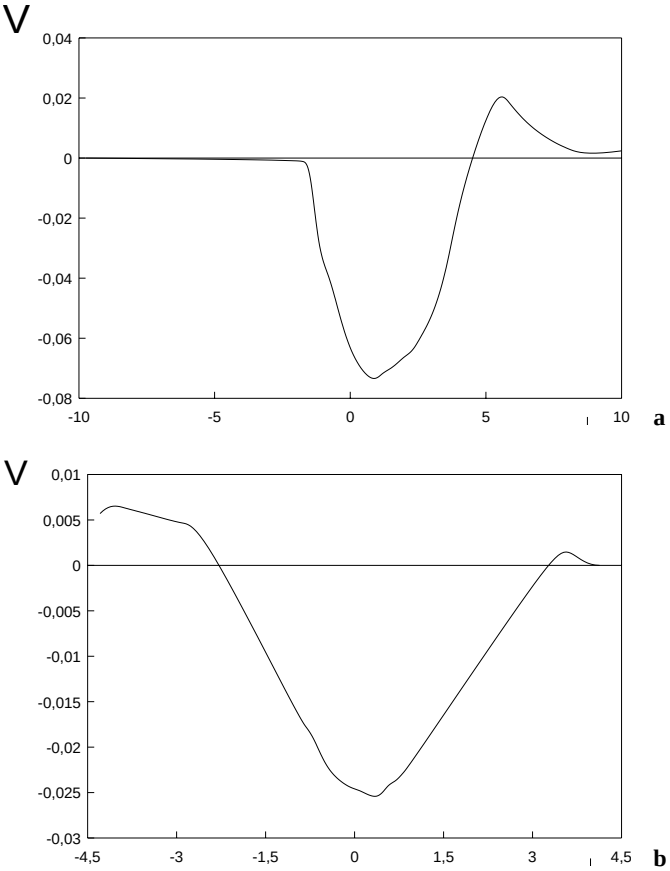

Fig. 5. The profiles of circular polarization given the efficient outward refraction at the outer edges of the open field line tube: **a** $\gamma = 50$, $f_0 = 0.5$, $\alpha = 1.2$, $\xi - \alpha = 0.017$, $r_f/r_L = 0.05$, $\frac{\omega r_f}{c\gamma^2} = 7.5$, $\chi_1 = 0.01$, $\chi_c = 5.5\chi_1$, $\chi_2 = 10\chi_1$, **b** the same parameters, save that $\chi_1 = 0.003$, $\chi_c = 6\chi_1$, $\xi - \alpha = 0.018$

by the observations. Indeed, the lack of circular polarization in conal components is a well-known observational fact (see, e.g., Rankin 1983). The V-profiles, in which the circular polarization changes sense at the periphery are also quite abundant, especially in the high-frequency reviews (see, e.g., Rankin et. al. 1989).

Although the theory of polarization-limiting effect because magnetosphere rotation is worked out sufficiently minutely (Cheng & Ruderman 1979; Stinebring 1982; Barnard 1986; Lyubarskii & Petrova 1999), so far there is no reliable estimate of the polarization-limiting radius. The point is that r_p turns out to be essentially dependent on a number of parameters, which can vary within some orders of magnitude. In addition, the value of r_p depends crucially upon the angle the wave vector makes with the magnetic field, which is in turn determined by the structure of the magnetosphere. Unfortunately, up to date there is no self-consistent quantitative description of the rotating magnetosphere containing the plasma. So one cannot firmly specify the locus of the polarization-limiting radius in the magnetosphere and we treated it as a free parameter. However, it is r_p that conditions the final value of the circular polarization in the case considered. As r_p is near the emission region, $r_p \sim r_0$, rotation effect is weak and the emergent circular polarization is small. Polarization-limiting effect taking place at large distances, $r_p \sim r_L$, also results in a weak circular polarization, since in the outer magnetosphere the turn of the $\mathbf{k} \times \mathbf{b}$-plane along the trajectory ceases. The variety of the maximum values of circular polarization observed in the symmetrical V-profiles testifies for the variety of conditions in pulsar magnetospheres. Due to the lack of a reliable expression for r_p, it is not possible to say anything about the evolution of the symmetrical V-profiles with the frequency. Note that in reality both trends of the frequency evolution are observed (see, e.g., Manchester, Hamilton, McCulloch 1980).

3.3. The swing of position angle of linear polarization with allowance for wave mode coupling

The polarization of normal waves originating in the magnetospheric plasma is certainly connected with the local orientation of the magnetic field. So the position angle of linear polarization should vary as the sight line traverses the open field line tube. Given that the propagation effects are ignored, the position angle swing through the pulse is known to be S-shaped (e.g., Manchester & Taylor 1977). Wave propagation in the vicinity of the emission region can be treated in terms of geometrical optics. The wave polarization then follows the local orientation of the $\mathbf{k} \times \mathbf{b}$-plane. Barnard (1986) was the first to investigate the influence of this effect on the observed position angle swing. It was found that given $r_p \sim r_L$ the total swing through the pulse should be essentially diminished. Note that polarization transfer in the polarization-limiting region, where geometrical optics approximation is violated, is also expected to result in position angle variation. Indeed, at distances $\sim r_p$ wave polarization has not enough time to follow the $\mathbf{k} \times \mathbf{b}$-plane turn and the waves suffer birefringence. Then the polarization becomes elliptical, with the polarization ellipse turning along the trajectory. So the polarization-limiting effect influences the position angle swing as well as produces the circular polarization in the outgoing radiation. It should be pointed out that irregular position angle swing and large amounts of circular polarization are really observed together, both being the attributes of the so-called core emission (e.g., Rankin 1990). In the present subsection we are to study the position angle swing across the pulse taking into account wave propagation in the polarization-limiting region.

If the position angle, μ, were determined by the orientation of the magnetic field, it would be presented as follows (Barnard & Arons 1986; Barnard 1986):

$$\tan\mu = [1 - (\mathbf{b}\cdot\mathbf{\Omega})^2 - (\mathbf{n}\cdot\mathbf{b})^2 - (\mathbf{n}\cdot\mathbf{\Omega})^2$$

$$+2(\mathbf{n}\cdot\mathbf{b})(\mathbf{n}\cdot\mathbf{\Omega})(\mathbf{\Omega}\cdot\mathbf{b})]^{1/2}[(\mathbf{b}\cdot\mathbf{\Omega})$$

$$-(\mathbf{n}\cdot\mathbf{b})(\mathbf{n}\cdot\mathbf{\Omega})]^{-1}. \qquad (22)$$

This can be easily reduced to the form (see also Manchester & Taylor 1977):

$$\tan\mu = \frac{\sin\alpha\sin\Phi}{\sin\xi\cos\alpha - \cos\xi\sin\alpha\cos\Phi}$$

$$\approx \frac{\Phi \sin\alpha}{\xi - \alpha} \equiv -\tan\varphi. \quad (23)$$

Generally the position angle should be determined by the direction of the major axis of polarization ellipse, $\mathbf{l}$, beyond the polarization-limiting region. Then, taking into account that the waves considered are transverse ones, i.e. $\mathbf{l}\cdot\mathbf{n} \equiv 0$, one can rewrite Eq. (22) as

$$\tan\mu = \frac{\sqrt{1-(\mathbf{l}\cdot\mathbf{\Omega})^2-(\mathbf{n}\cdot\mathbf{\Omega})^2}}{(\mathbf{l}\cdot\mathbf{\Omega})}. \quad (24)$$

Following Landau & Lifshits (1988), one can express the components of the vector $\mathbf{l}$ via the wave amplitudes a_x and a_y. The wave electric field can be presented in the form:

$$\mathbf{E} = (a_{x1}+ia_{x2})\mathbf{i} + (a_{y1}+ia_{y2})\mathbf{j}$$

$$= (\mathbf{l}_1 + i\mathbf{l}_2)e^{-i\delta}, \quad (25)$$

where $a_{x1}+ia_{x2} \equiv a_x$, $a_{y1}+ia_{y2} \equiv a_y$, $\mathbf{l}_1$ and $\mathbf{l}_2$ are the principal axes of the polarization ellipse, so that $\Im(\mathbf{l}_1+i\mathbf{l}_2)^2 = 0$. Proceeding from the equality:

$$\Re\{(\mathbf{E}\cdot\mathbf{l}_1)(\mathbf{E}^*\cdot\mathbf{l}_2)\} = 0, \quad (26)$$

where the complex conjugation is marked by asterisk, it is easy to find the inclination ϑ of the major axis $\mathbf{l}_1$ to the x-axis ($\tan\vartheta \equiv l_{1y}/l_{1x}$):

$$\tan 2\vartheta = \frac{2(a_{x1}a_{y1}+a_{x2}a_{y2})}{a_{x1}^2+a_{x2}^2-a_{y1}^2-a_{y2}^2}. \quad (27)$$

Taking into account that

$$\mathbf{n}\cdot\mathbf{\Omega} = \cos\xi \approx \cos\alpha,$$

$$\Omega_x = -\sin\alpha\cos\varphi - \theta\cos\alpha,$$

$$\Omega_y = \sin\alpha\sin\varphi,$$

we obtain finally:

$$\tan\mu = \frac{\sqrt{1-[\cos(\varphi+\vartheta)-\theta\cot\alpha\cos\vartheta]^2}}{\cos(\varphi+\vartheta)-\theta\cot\alpha\cos\vartheta}. \quad (28)$$

Using in Eq. (27) the limiting values of the wave amplitudes found through the numerical solution of Eqs. (17) and (13) yields the curves of position angle swing presented in Fig. 6. The swing without allowance for the polarization-limiting effect is shown by the dashed lines. The swing in Fig. 6a is obtained at the same parameters as the V-profile in Fig. 3b. One can see that under such condition the polarization-limiting effect does not alter essentially the character of the swing. Position angle variation remains quite smooth, the total swing through the pulse being almost the same. The value of the total swing is close to $180°$ implying that the sight line traverses the open field line tube close enough to the centre. Obviously, at a fixed $|\alpha-\xi|$ the smaller the pulse width the larger is the normalized impact parameter $|\alpha-\xi|/\theta_{max}$. As clear from Fig. 6a, in case

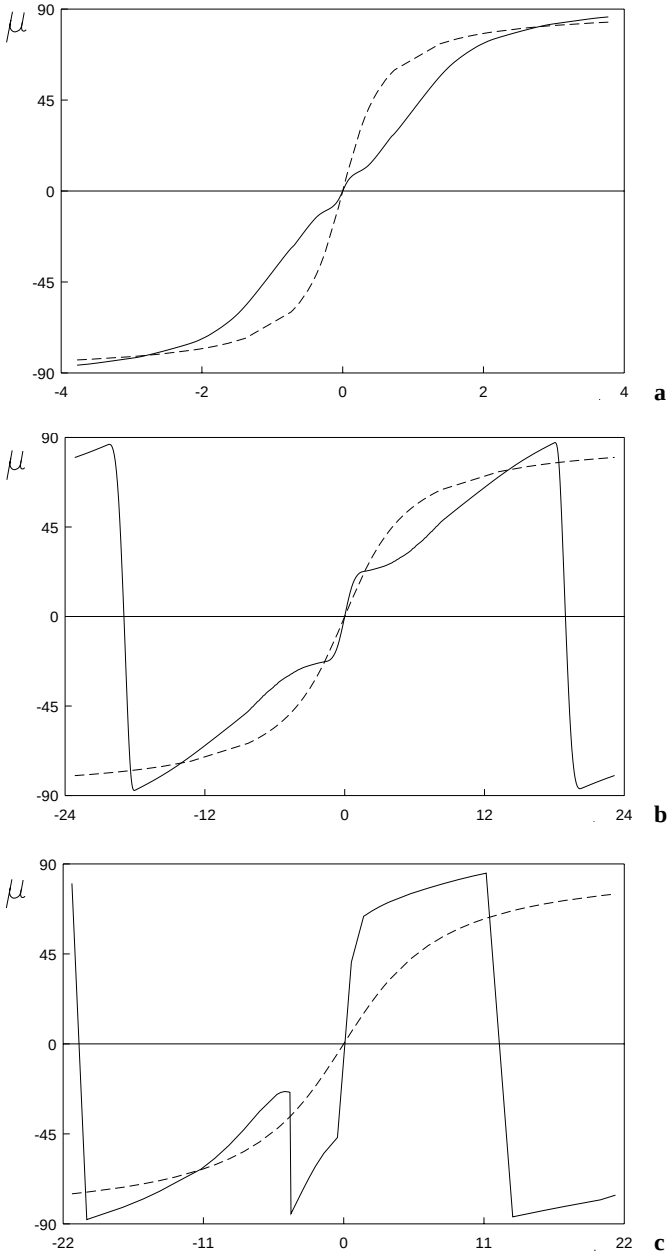

Fig. 6. The swing of position angle of linear polarization with allowance for wave propagation in the polarization-limiting region: **a** $\alpha = 0.5$, **b** $\alpha = 0.05$; the rest parameters are the same as on Fig. 1b, **c** the parameters are the same as on Fig. 4

of non-central sight-line trajectories the polarization-limiting effect something diminishes the total position angle swing. Position angle variation shown in Fig. 6a is similar to that observed for some pulsars with the antisymmetric V-profiles (e.g., PSR 1508+55, PSR 2111+46, and PSR 0942-13 (Lyne & Manchester 1988)).

If one considers another parameter, the influence of polarization-limiting effect on the position angle swing can be more significant (see Fig. 6b). One can see that the transition in the pulse centre becomes more distinct and the total swing exceeds $180°$. The latter is really the case in some pulsars.

The abrupt change of position angle near the pulse centre corresponding to the sense reversal in V-profile is observed, e.g., for PSR 1451-68 (McCulloch et. al. 1978).

Fig. 6c shows the position angle variation in case of symmetrical V-profile. The essential departure from the S-shape corresponds to the peak of V-profile. It should be mentioned that as a rule the position angle swing observed in the conal components of triple profiles is smooth and can be regarded as the S-shaped, whereas the swing in the central components can be quite irregular, usually with abrupt transitions, which are not necessarily orthogonal (see, e.g., McCulloch et. al. 1978, Rankin et. al. 1989). So in the whole position angle swing presented in Fig. 6c also agrees with the observations.

3.4. Interpretation of total-intensity profiles in terms of refraction

The hollow-cone model (Radhakrishnan & Cooke 1969) is commonly accepted as a basis for geometrical explanation of pulsar total-intensity profiles. From the physical point of view, pulsar radio emission is associated with the magnetospheric plasma, which is believed to be distributed within the open field line tube, with the density close to the magnetic axis being negligible. Given the radius-to-frequency mapping is the case the widening of double profiles with the wavelength as well as the increase of separation between the components are naturally explained by the open field line tube widening with the distance from the neutron star. However, as first established by Backer (1976), in addition to the basic double structure the observed profiles often contain the component near the pulse centre, whereas some profiles exhibit two pairs of almost symmetrical components near the central component. So the hollow-cone model called for modification.

Thorough analysis of the wide observational data led Rankin (1983) to the conclusion that the emission from the central part of the open field line tube (core emission) differs from that generated at the tube edges (conal emission) in physical properties, namely in polarization and spectral behaviour. Later on Lyne & Manchester (1988) argued for a smooth variation of these properties with the distance from the magnetic axis, without respect to the concrete components of total-intensity profiles. In the previous subsections we demonstrated that the propagation effects in pulsar magnetosphere can account for both considerable circular polarization and irregular position angle swing close to the pulse centre, whereas the emission at the wings should be characterized by small amounts of circular polarization and quite orderly swing. This is well compatible with the observations.

Now we turn to the spectral properties of pulsar total-intensity profiles. As found out by Rankin (1983), core components have a steeper spectrum than the conal ones, so that at high frequencies the conal emission becomes more prominent. The frequency evolution of triple profiles was well simulated theoretically in terms of purely geometrical effects (Sieber 1997). The author proceeded from the assumption that pulsar emission beam contained a gaussian beam centered on the magnetic axis as well as shifted gaussian beams corresponding to conal emission. Our aim is to suggest the physical basis for such geometrical considerations. We are to show that refraction in the magnetospheric plasma can provide the separation of pulse components. Note that the beam separation on account of refraction should be frequency-dependent.

Consider refraction in the plasma with the following density distribution:

$$N=\begin{cases} N_0\left(\frac{r_0}{r}\right)^3\left(\frac{\chi-\chi_1\sqrt{r/r_0}}{(\chi_c-\chi_1)\sqrt{r/r_0}}\right)^2, & \chi_1\sqrt{\frac{r}{r_0}}\le\chi\le\chi_c\sqrt{\frac{r}{r_0}},\\ N_0\left(\frac{r_0}{r}\right)^3\left(\frac{\chi_2\sqrt{r/r_0}-\chi}{(\chi_2-\chi_c)\sqrt{r/r_0}}\right)^2, & \chi_c\sqrt{\frac{r}{r_0}}\le\chi\le\chi_2\sqrt{\frac{r}{r_0}},\\ 0, \qquad \chi<\chi_1\sqrt{r/r_0} \quad \text{and} \quad \chi>\chi_2\sqrt{r/r_0}, \end{cases} \tag{29}$$

Let the emission be generated in the region filled with the plasma and radius-to-frequency mapping be the case. For simplicity we assume that the intensity distribution is uniform. Since the plasma number density decreases towards the both boundaries of the plasma flow, the transverse density gradient should change the sign. Then the rays emitted near the inner edge of the plasma flow should deviate towards the magnetic axis, while those emitted near the outer tube edge should tend away from the axis. Thus, refraction really leads to the angular separation of uniformly emitted radiation. At high frequencies refraction is more efficient (the tube is narrower and transverse density gradient is larger) and the component separation should become more distinct.

Using Eq. (29) in Eq. (7) one can find the total-intensity profiles shown in Fig. 7. They are obtained for the set of tube widths, that is for the set of frequencies related to each other as $1 : 1.37 : 1.95 : 2.32 : 2.92 : 3.64$. Note that the profiles in Fig. 7 are calculated at the assumption of the uniform intensity distribution throughout the emission region, while in reality it is not so. It is apparent that refraction in the hollow-cone beam causes the triplicity of the observed profiles, with the component separation becoming more distinct at higher frequencies. Note that at proper conditions refraction can split the hollow-cone beam into the five components (see Fig. 7f). The inner conal components are then formed by the rays emitted at $\chi \lesssim \chi_c$. The trajectories of such rays intersect the critical field line, so that the rays get finally into the region with the oppositely directed density gradient and suffer a slight deviation towards the outer tube edge. It should be mentioned that the five-component profiles are the most typical among the observed multiple profiles. Given that the inner boundary of the plasma flow lies far enough from the magnetic axis and the sight-line trajectory across the pulsar beam is sufficiently central, the central component can turn into a pair of components. So the recently discovered six-component profiles of PSR 0329+54 (Kuzmin & Izvekova 1996) and PSR 1237+25 (Kuzmin et al. 1997) can also be explained in the spirit of the present discussion. Thus the whole variety in the morphology of pulsar total-intensity profiles can be interpreted in terms of the common hollow-cone model with allowance for

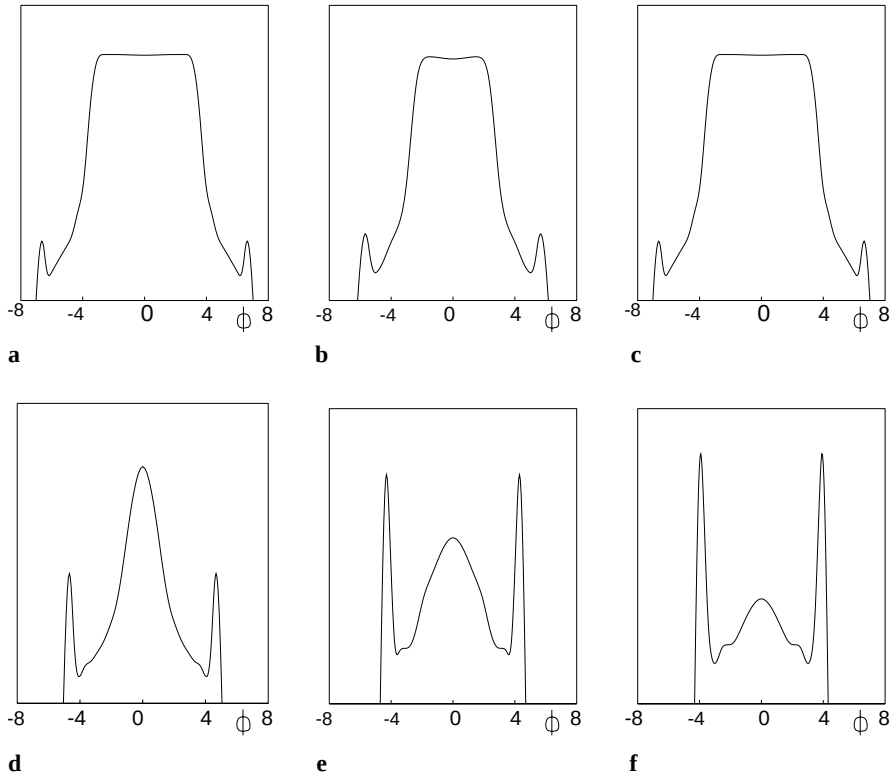

Fig. 7. The separation of components in total-intensity profiles due to refraction: **a** $\chi_1 = 0.01$, **b** $\chi_1 = 0.009$, **c** $\chi_1 = 0.008$, **d** $\chi_1 = 0.0075$, **e** $\chi_1 = 0.007$, **f** $\chi_1 = 0.0065$; $\gamma = 50$, $f_0 = 0.5$, $\xi - \alpha = 3.7^\circ$, $\chi_c = 6\chi_1$, $\chi_2 = 7\chi_1$

refraction in the magnetospheric plasma.

4. Conclusions

We investigated refraction and polarization transfer in an ultra-relativistic pulsar plasma embedded in an infinitely strong magnetic field. In agreement with the standard models of electron-positron cascade, the plasma density was assumed to be zero near the magnetic axis and beyond the boundary of the open field line tube. In addition, the plasma density distribution was taken to be nonaxisymmetric. This does not conflict with the customary model of magnetosphere structure. With such density distribution wave mode coupling introduced by refraction results in an antisymmetric profile of circular polarization with the sense reversal near the pulse centre. The observed frequency evolution of the antisymmetric V-profiles (the increase of $|V|$ with the frequency) corresponds to the increasing role of refraction at high frequencies. At low frequencies, which are believed to originate at high altitudes in the open field line tube, rotation effect is essential rather than refraction. Wave mode coupling introduced by magnetosphere rotation leads to symmetric profiles of circular polarization. The rays emitted sufficiently close to the edge of the open field line tube can intensely deviate out of the tube causing depolarization or even sense reversal at the wings of V-profile. The observed irregularities in the swing of position angle, which usually accompany high circular polarization, are also naturally explained by polarization-limiting effect.

We also suggested the interpretation of the morphological features of pulsar total-intensity profiles on the basis of propagation effects in the magnetosphere. It is shown that refraction in the plasma, whose number density decreases towards the magnetic axis and towards the edge of the open field line tube, can account for the angular separation of profile components. The spectral evolution of total-intensity profiles is well explained by the increasing efficiency of refraction at high frequencies.

In our investigation the plasma was assumed to be cold, although this is not the case in pulsar magnetospheres. It should be noted that the dispersive curves for the waves in the hot plasma are qualitatively similar to those in the case of the cold plasma (Lyubarskii 1995). The quantitative description of the waves in the hot plasma requires using the concrete form of the particle distribution function, which is still obscure. In addition, the exact distribution of the plasma number density across the open field line tube is also unknown. So the obtained results can allow some quantitative modification, while the qualitative picture is believed to remain the same.

References

Arons J.J., Scharlemann E.T., 1979, ApJ 231, 854
Backer D.C., 1976, ApJ 209, 895
Barnard J.J., 1986, ApJ 303, 280
Barnard J.J., Arons J., 1986, ApJ 302, 138
Biggs J.D., Lyne A.G., Hamilton P.A., et al., 1988, MNRAS 235, 255
Bjornsson C.I., 1984, ApJ 277, 367
Cheng A.F., Ruderman M.A., 1979, ApJ 229, 348
Gangadhara R.T., 1997, A&A 327, 155
Gil J.A., Snakowski J.K., 1990a, A&A 234, 237

Gil J.A., Snakowski J.K., 1990b, A&A 234, 269
Han J.L., Manchester R.N., Xu R.X., Qiao G.J., 1998, MNRAS 300, 373
Kuzmin A.D., Izvekova V.A., 1996, Pis'ma v Astron. Zh. 22, 439
Kuzmin A.D., Losovskii B.Ya., Lapaev K.A., 1997, Proceedings of the XXVII Radioastronomy Conference 1, St.Petersburg, 237
Landau L.D., Lifshits Ye.M., 1988, The Classical Theory of Fields. Nauka, Moscow
Lyne A.G., Manchester R.N., 1988, MNRAS 234, 477
Lyubarskii Yu.E., 1995, Astrophys. Space Phys. Rev. vol. 9, pt. 2, p. 1
Lyubarskii Yu.E., Petrova S.A., 1998, A&A 333, 181
Lyubarskii Yu.E., Petrova S.A., 1999, Ap&SS, 262, 379
Manchester R.N., Taylor J.H., 1977, Pulsars. W.H. Freeman and Company, San Francisco
Manchester R.N., Hamilton P.A., McCulloch P.M., 1980, MNRAS 192, 153
McCulloch P.M., Hamilton P.A., Manchester R.N., Ablels J.G., 1978, MNRAS 183, 645
Michel F.C., 1987, ApJ 322, 822
Radhakrishnan V., Cooke D.J., 1969, ApJ 3, L225
Radhakrishnan V., Rankin J.M., 1990, ApJ 352, 258
Rankin J.M., 1983, ApJ 274, 333
Rankin J.M., 1990, ApJ 352, 247
Rankin J.M., Benson J.M., 1981, AJ 86, 418
Rankin J.M., Stinebring D.R., Weisberg J.M., 1989, ApJ 346, 869
Sieber W., 1997, A&A 321, 519
Stinebring D.R., 1982, Ph.D. Thesis, Cornell University
von Hoesbroech A., Lesch H., Kunzl T., 1998, A&A 336, 209